Mantle–slab interaction and redox mechanism of diamond formation

Yuri N. Palyanov[a,b,1], Yuliya V. Bataleva[a,b], Alexander G. Sokol[a,b], Yuri M. Borzdov[a], Igor N. Kupriyanov[a], Vadim N. Reutsky[a], and Nikolai V. Sobolev[a,1]

[a]V.S. Sobolev Institute of Geology and Mineralogy Siberian Branch Russian Academy of Sciences, Novosibirsk 630090, Russia; and [b]Geology and Geophysics Department, Novosibirsk State University, Novosibirsk 630090, Russia

Edited by Ho-kwang Mao, Carnegie Institution of Washington, Washington, DC, and approved November 1, 2013 (received for review July 15, 2013)

Subduction tectonics imposes an important role in the evolution of the interior of the Earth and its global carbon cycle; however, the mechanism of the mantle–slab interaction remains unclear. Here, we demonstrate the results of high-pressure redox-gradient experiments on the interactions between Mg-Ca-carbonate and metallic iron, modeling the processes at the mantle–slab boundary; thereby, we present mechanisms of diamond formation both ahead of and behind the redox front. It is determined that, at oxidized conditions, a low-temperature Ca-rich carbonate melt is generated. This melt acts as both the carbon source and crystallization medium for diamond, whereas at reduced conditions, diamond crystallizes only from the Fe-C melt. The redox mechanism revealed in this study is used to explain the contrasting heterogeneity of natural diamonds, as seen in the composition of inclusions, carbon isotopic composition, and nitrogen impurity content.

carbonate–iron interaction | high-pressure experiment | mantle mineralogy | deep carbon cycle

Subduction of crustal material plays an important role in the global carbon cycle (1–6). Depending on oxygen fugacity and pressure-temperature (P-T) conditions, carbon exists in the Earth's interior in the form of carbides, diamond, graphite, hydrocarbons, carbonates, and CO_2 (7–11). In the upper mantle, the oxygen fugacity (fO_2) varies from one to five log units below the fayalite-magnetite-quartz (FMQ) buffer, with a trend of a decrease with depth (6, 12–15). At a depth of ∼250 km, mantle is reported to become metal saturated (16, 17), which holds true for all mantle regions below, including the transition zone and lower mantle. The subduction of the oxidized crustal material occurs to depths greater than 600 km (4–6). The main carbon-bearing minerals of the subducted materials are carbonates, which are thermodynamically stable up to P-T conditions of the lower mantle (10, 11, 18). As evidenced by the compositions of inclusions in diamond, which vary from strongly reduced, e.g., metallic iron and carbides (19–23), to oxidized, e.g., carbonates and CO_2 (6, 20, 24–28), carbonates may be involved in the reactions with reduced deep-seated rocks, including Fe^0-bearing species (29–31). A scale of these reactions is determined mainly by the capacity of subducted carbonate-bearing domains. An important consequence of such an interaction is that it can produce diamond. However, studies on diamond synthesis via the reactions between oxidized and reduced phases are limited (32–35).

To understand the mechanisms of the interaction of carbon-bearing oxidized- and reduced-mineral assemblages, we performed high-pressure experiments with an iron-carbonate system; an approach was used that enabled the creation of an oxygen fugacity gradient in the capsules (*Materials and Methods* and *SI Materials and Methods*).

Results and Discussion

The experimental results and the phase compositions are given in Table 1 and Table S1, respectively. At temperatures of 1,000 and 1,100 °C, the iron–carbonate interaction can be described, in general, by the reaction

$$(Mg, Ca)CO_3 + Fe^0 \rightarrow (Fe, Mg)O + Fe_3C + (Ca, Mg, Fe)CO_3 + C^0. \quad [1]$$

Iron carbide (Fe_3C, cohenite) in the above reaction is formed on saturation of the iron with reduced carbon. This iron carbide further reacts with the initial carbonate to produce an association of magnesiowustite + metastable graphite + Ca-rich carbonate. Finally, in the central (reduced) part of the capsules, Fe_3C is produced, which is surrounded by a reaction zone (Fig. 1*A*), consisting of carbide, graphite, and magnesiowustite. The magnesiowustite exhibits an increase in the Mg number (Mg#) from 0.13 at the contact with carbide to 0.37 at the periphery of the zone. In the outer (oxidized) part of the capsules, an assembly of magnesiowustite (Mg# = 0.38), aragonite (Ca# = 0.89), and graphite (Fig. 2*A*) is formed. When cohenite was used as the starting material instead of iron, the character of the interaction did not change, but the amount of graphite significantly increased.

At 1,200 °C and higher temperatures, a Ca-rich carbonate melt coexisting with almost Ca-free magnesiowustite and ferromagnesite was present in the system. On quenching, this melt crystallized to dendritic aggregates of Ca,Mg,Fe carbonates and magnesiowustite (Figs. 1 *B* and *D* and 2 *B–E*). A notation $[CaCO_3 + (Fe,Mg)O]_L$ will further be used to designate the Ca-rich carbonate melt with dissolved magnesiowustite. As a result of the redox reaction, metallic iron extracts carbon from carbonate to form carbide. A reaction zone, consisting of high-Fe magnesiowustite, Fe_3C, and graphite is formed around the carbide (Fig. 2*F*). Cohenite

Significance

The primary question that we address in this study is what happens when a carbonate-bearing crust is subducted to depths where the Earth's mantle is metal saturated. Subduction plays an important role in the evolution of the Earth's interiors, but the mechanism of the interaction between the oxidized slab and reduced mantle remains unclear. Here we report the results of high-pressure redox-gradient experiments on the interaction between Mg-Ca-carbonate and metallic iron, modeling the processes at the mantle–slab boundary, and present mechanisms of diamond formation ahead of and behind the redox front. We demonstrate that the redox mechanism revealed in this study can explain the contrasting heterogeneity of natural diamonds on the composition of inclusions, carbon isotopic composition, and nitrogen impurity content.

Author contributions: Y.N.P. and N.V.S. designed research; Y.N.P., Y.V.B., A.G.S., and Y.M.B. performed research; I.N.K. and V.N.R. contributed new reagents/analytic tools; Y.N.P., Y.V.B., A.G.S., Y.M.B., I.N.K., and V.N.R. analyzed data; and Y.N.P., Y.V.B., I.N.K., and N.V.S. wrote the paper.

The authors declare no conflict of interest.

This article is a PNAS Direct Submission.

[1]To whom correspondence may be addressed. E-mail: palyanov@igm.nsc.ru or sobolev@igm.nsc.ru.

This article contains supporting information online at www.pnas.org/lookup/suppl/doi:10.1073/pnas.1313340110/-/DCSupplemental.

Table 1. Experimental conditions and results

Run no.	*P*, GPa	*T*, °C	*t*, h	Initial composition, mg		Phase association of zones* (from center to periphery of samples)
				$Mg_{0,9}Ca_{0,1}CO_3$	Fe^0	
1567	6.5	1,350	20	440	507	[Coh, $(Fe\text{-}C)_L$] → [Coh, Mws, Gr] → [Mws, $(Carb+Mws)_L$, Gr] → [Fms, $(Carb+Mws)_L$, Dm, Dm*]
1250	6.5	1,450	20	340	700	[Coh, $(Fe\text{-}C)_L$] → [Coh, Mws, Gr, Dm] → [Mws, $(Carb+Mws)_L$, Gr, Dm] → [$(Carb+Mws)_L$, Mws, Gr, Dm]
1566	6.5	1,550	10	340	535	[Coh, $(Fe\text{-}C)_L$, Dm] → [Coh, Mws, Dm] → [Mws, $(Carb+Mws)_L$, Gr, Dm] → [$(Carb+Mws)_L$, Gr, Dm]
1571	6.5	1,600	8	440	494	[Coh, $(Fe\text{-}C)_L$, Dm] → [Coh, Mws, Dm] → [Mws, $(Carb+Mws)_L$, Gr,Dm] → [$(Carb+Mws)_L$, Gr, Dm]
1541	7.5	1,000	60	110	55	Coh → [Coh, Mws, Gr] → [Mws, Marg, Gr] → [Fms, Marg]
1540	7.5	1,100	60	110	53.9	[Mws, Marg, Gr] → [Fms, Marg, Gr]
1532	7.5	1,200	60	110	58	[Mws, $(Carb+Mws)_L$, Gr] → [Fms, $(Carb+Mws)_L$, Mws, Gr, Dm**]
1528	7.5	1,300	60	130	80	[Mws, $(Carb+Mws)_L$, Gr, Dm] → [Fms, $(Carb+Mws)_L$, Mws, Gr, Dm, Dm**]
1525	7.5	1,400	60	130	78	[Mws, $(Carb+Mws)_L$, Gr, Dm] → [Fms, $(Carb+Mws)_L$, Mws, Gr, Dm, Dm**]
1517	7.5	1,450	30	140.1	59.1	[Mws, $(Carb+Mws)_L$, Gr, Dm] → [$(Carb+Mws)_L$, Mws, Fms, Gr, Dm]
1515	7.5	1,550	20	127.2	56.1	[Mws, $(Carb+Mws)_L$, Gr, Dm] → [$(Carb+Mws)_L$, Mws, Fms, Gr, Dm]
1521	7.5	1,650	8	140	75.8	[Mws, $(Carb+Mws)_L$, Dm] → [$(Carb+Mws)_L$, Fms, Dm]
				$Mg_{0,9}Ca_{0,1}CO_3$	Fe_3C	
1561	7.5	1,000	60	110	63	Coh → [Coh, Mws] → [Coh, Mws, Gr] → [Mws, Arg, Gr] → [Fms, Arg]
1560	7.5	1,100	60	110	57	Coh → [Coh, Mws] → [Coh, Mws, Gr] → [Mws, Arg, Gr] → [Fms, Arg]
1552	7.5	1,200	60	110	67	Coh → [Coh, Mws, Gr] → [Mws, $(Carb+Mws)_L$, Gr] → [Fms, $(Carb+Mws)_L$, Mws, Dm**]
1548	7.5	1,300	60	120	107	Coh → [Coh, Gr, Mws] → [Mws, $(Carb+Mws)_L$, Gr] → [$(Carb+Mws)_L$, Mws, Fms, Gr, Dm**]
1545	7.5	1,400	60	120	110	Coh → [Coh, Gr, Mws] → [Mws, $(Carb+Mws)_L$, Gr] → [Fms, $(Carb+Mws)_L$, Mws, Gr, Dm, Dm**]

*Compositions of phases from different zones are given in Table S1. Arg, aragonite; $(Carb+Mws)_L$, carbonate melt with dissolved magnesiowustite; Coh, cohenite (Fe_3C); Dm, diamond; Dm**, diamond growth on seeds; $(Fe\text{-}C)_L$, iron-carbon melt; Fms, ferromagnesite; Gr, graphite; Marg, Mg-aragonite; Mws, magnesiowustite.

reduces some carbon from the carbonate melt, according to the reaction

$$(Ca, Mg, Fe)CO_{3(L)} + Fe_3C \rightarrow (Fe, Mg)O + [CaCO_3 + (Fe, Mg)O]_L + C^0. \quad [2]$$

Thus, in the center, where carbide and the reaction zone (Mws + Coh + Gr) are present, the fO_2 values correspond approximately to that of the iron-wustite (IW) buffer (about FMQ-5 log units). In the peripheral part of the capsules, where the magnesiowustite + carbonate melt + C^0 association is formed, fO_2 corresponds to values characteristic of magnesiowustite-poor carbonate melt in equilibrium with graphite or diamond (about FMQ-1 log unit) (14). Therefore, at the initial stages of the interaction, the oxygen fugacity gradient over the capsules is nearly 4 log units. As a consequence, a redox front arises at the iron/carbonate boundary. As the interaction progresses, the fO_2 gradient in the capsules gradually decreases. A reconstructed scheme of the iron-carbonate interaction is shown in Fig. 3. The exchange between the oxidized periphery and reduced center involves a fluid and Ca-rich carbonate melt, capable of dissolving and transporting a significant amount of magnesiowustite. In this process, the melt is partly consumed to form magnesiowustite and elemental carbon. The rate of the iron–carbonate interaction can be estimated by the width of the reaction zone containing magnesiowustite. It was determined that the fronts of the iron–carbonate and carbonate–cohenite reactions propagate at similar rates, which increase from 6.7 to 14.8 μm/h as the temperature increases from 1,000 °C to 1,400 °C, respectively, at 7.5 GPa. The redox interaction ceases when Fe_3C is completely consumed.

The compositions of the final phases and their trends are shown in Table S1 and Fig. 4. The Mg# of magnesiowustite and ferromagnesite, coexisting with the carbonate melt, increases with temperature. An increase in temperature, and thus the degree of partial melting, leads to a decrease in Ca# of the carbonate melt. Analyses of the quench aggregate show that the carbonate melt can dissolve a significant amount of magnesiowustite, as high as 15 wt.% at 1,200 °C and up to 22 wt.% at 1,650 °C.

The formation of elemental carbon (graphite and diamond) through the iron–carbonate redox interaction deserves special consideration. In most experiments, as a result of the oxidation of iron carbide, metastable graphite in association with magnesiowustite is formed in the central zone (Fig. 2 *D* and *E*). Crystallization of graphite rather than diamond can be accounted for by the absence of the solvent, as well as by the P-T conditions insufficient for the direct graphite-to-diamond transformation. Finally, in most experiments after complete exhaustion of cohenite, a graphite lens (Fig. 1*C*) with inclusions of carbide in association with magnesiowustite remains in the center of the samples. However, in some experiments at temperatures ≥1,450 °C (Table 1), a quenched metal melt with relatively large (up to 1 mm) diamond crystals (Fig. 5) occurred. The number of diamond nucleation centers is rather small (10^{-1}/mm^3), and the growth rate is ~40 μm/h. Crystallization of these diamonds is associated with the appearance of a metal-carbon melt, which arises due to the existence of the metastable Fe-graphite eutectic (8, 36). At the initial stages of the interaction, the iron is gradually saturated with carbon to form metal-carbon melt and carbide. If graphite is in contact with the metal melt, nucleation of diamond occurs. As iron reacts with carbonate, the metal melt saturates with carbon, and the iron is gradually consumed by oxidation. Thereby, carbon supersaturation is established in the residual melt, which facilitates further growth of the diamond. A similar mechanism possibly operates in the micropools of metal melt, located in the reaction zone containing magnesiowustite. In this case, diamond

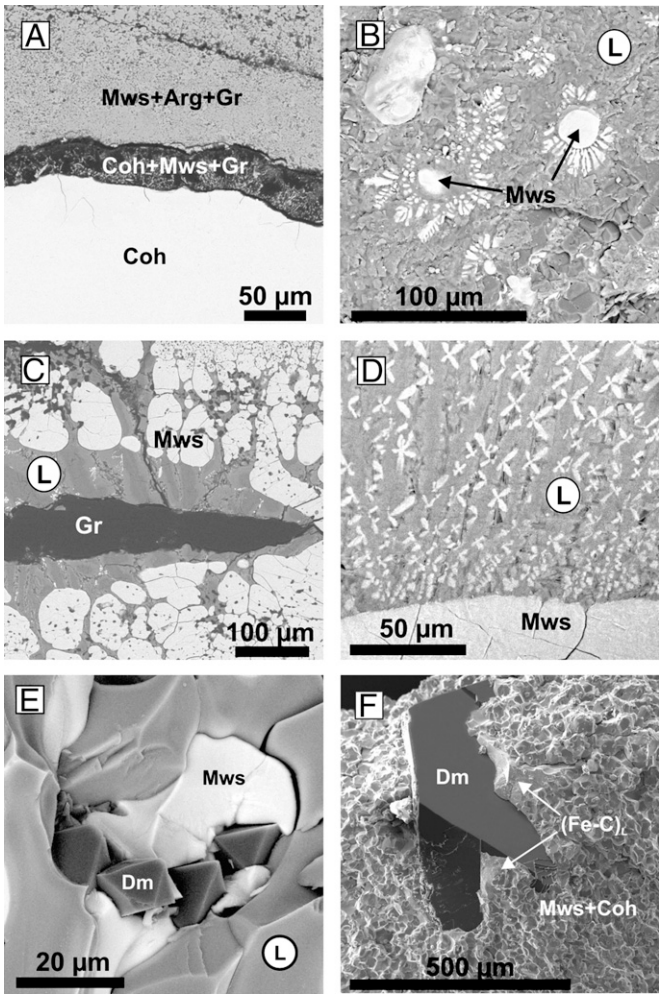

Fig. 1. SEM micrographs: (*A*) reaction zone (cohenite + magnesiowustite + graphite) (N 1541); (*B*) magnesiowustite crystals in a dendritic aggregate of quenched carbonate and magnesiowustite (N 1521); (*C*) lens of metastable graphite in a dendritic aggregate of carbonate and magnesiowustite (N 1517); (*D*) dendritic aggregate of carbonate and magnesiowustite (N 1532); (*E*) diamond and magnesiowustite in quenched carbonate melt (N 1515); (*F*) diamond in polycrystalline aggregates of magnesiowustite, cohenite, and quenched iron-carbon melt (N 1566). Coh, cohenite (Fe_3C); Mws, magnesiowustite; L, carbonate melt with dissolved magnesiowustite; $(Fe\text{-}C)_L$, iron-carbon melt; Arg, aragonite; Gr, graphite; Dm, diamond.

microcrystals (3–5 μm in size) and their aggregates are formed. Finally, the metal-carbon melt is consumed completely and replaced with diamonds, in association with magnesiowustite. It is important to note that in experiments where Fe_3C was used instead of Fe^0 as the starting material, no metal-carbon melt was generated, and consequently, no diamonds were seen to form ahead of the redox front.

Behind the redox front, in the oxidized conditions, diamond growth on the seeds in the carbonate melt is established at temperature as low as 1,200 °C. At 1,300 °C, spontaneous growth of diamond crystals occurs on the seeds, which demonstrates heterogeneous nucleation. At temperatures ≥1,400 °C, homogeneous nucleation of diamond takes place (Fig. 5). With increasing temperature from 1,200 °C to 1,650 °C, the average diamond growth rate increases from 0.04 to 2 μm/h, respectively. The number of diamond nuclei in the carbonate melt increases from tens to hundreds per cubic millimeter as the temperature increases from 1,400 °C to 1,650 °C. The formation of diamond from the carbonate melt can generally be described by reaction **2**. These diamonds grew through the carbon reduction from the carbonate melt, as long as the Fe_3C was present in the capsule. New diamonds nucleate near the interface between the interacting Fe_3C and carbonate melt. When the Fe_3C is completely consumed, redox reaction **2** ceases, but a significant amount of carbon in the form of metastable graphite remains in the central part of the capsule. Therefore, in prolonged experiments, diamond growth continues owing to the transport of carbon dissolved in the carbonate melt, along with the recrystallization of magnesiowustite. Thus, we can conclude that the carbonate melt, generated in the course of the carbonate–iron interaction at temperatures ≥1,200 °C, plays a key role in the formation of diamond, being both a crystallization medium and the source of carbon.

Infrared absorption measurements show that diamond crystals synthesized in the metal-carbon melt contain 100–200 atomic ppm of nitrogen impurity in the form of single substitutional atoms (C-centers; Fig. 5). Inclusions of the quenched Fe-C melt are typical of these crystals. Diamonds, formed in the carbonate melt, exhibit significantly higher nitrogen concentrations ranging from 1,000 to 1,500 ppm. Nitrogen in this case is present mainly

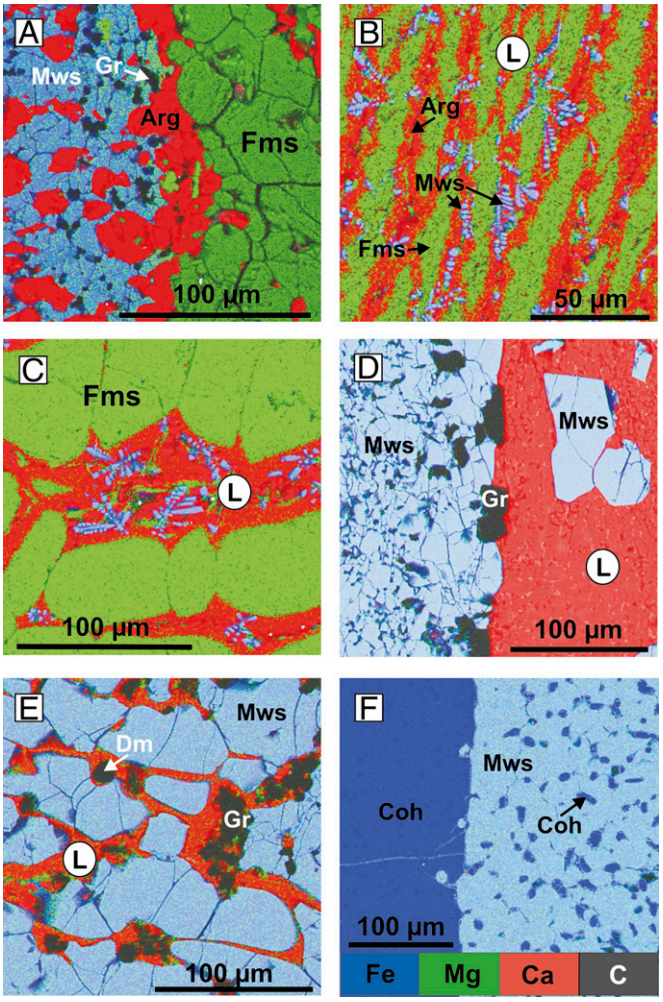

Fig. 2. SEM micrographs of representative phase assemblages, combined with compositional maps: (*A*) magnesiowustite + aragonite + graphite at the contact with ferromagnesite (N 1541); (*B*) dendritic aggregate of carbonates and magnesiowustite (N 1515); (*C*) ferromagnesite in carbonate melt (N 1517); (*D*) magnesiowustite and metastable graphite in carbonate melt (N 1250); (*E*) magnesiowustite, metastable graphite, and diamond in carbonate melt (N 1525); (*F*) reaction zone (cohenite + magnesiowustite) (N 1250). Fms, ferromagnesite.

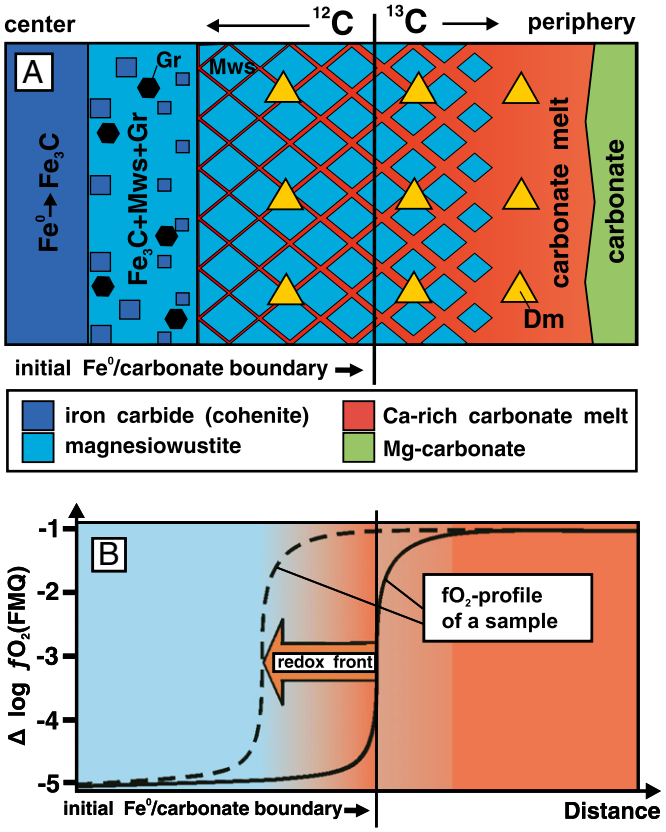

Fig. 3. A scheme of the iron–carbonate interaction, illustrating the mechanism of redox front formation via fO_2 gradient: (*A*) distribution of phases in a sample; (*B*) fO_2 profiles in a sample at the initial stage (solid line) and at a certain moment of the redox interaction (dashed line). Arrow denotes direction of the redox front propagation.

as C-centers, but for diamonds crystallized at higher temperatures (>1,500 °C) with considerable run duration (20 h), a significant portion of nitrogen (30–40%) occurs in the aggregated form, as nitrogen pairs or the so-called A-centers. In addition, absorption spectra frequently showed an absorption peak at ~1,440–1,450 cm^{-1}, which is associated with carbonate inclusions, and a weak peak at 3,107 cm^{-1}, which is due to hydrogen-related defects (Fig. 5). It is interesting to note that, whereas the nitrogen content of ~200 ppm is typical for most synthetic diamonds produced from metal–carbon systems, concentrations of around 1,000 ppm is normal for natural type Ia diamonds.

Carbon isotope analysis reveals that the starting carbonate has $\delta^{13}C = +0.2$ ‰, relative to the Pee Dee Belemnite (PDB) standard. The iron carbide formed in the reduced part of the capsules at 6.5 GPa and temperatures of 1,350 °C, 1,450 °C, and 1,550 °C has $\delta^{13}C$ of –3.7‰, –5.9‰, and –5.0‰, respectively. The carbonate melt, which is present in the oxidized part of the capsules, is enriched in the heavy carbon isotope and has $\delta^{13}C = +2.1$‰ (1,350 °C), +1.7‰ (1,450 °C), and +1.4 ‰ (1,550 °C). Thus, the isotope fractionation, accompanying the formation of iron carbide from the carbon of carbonate, has an average magnitude of 6.5‰.

The interaction of carbonate with Fe^0 is considered a simplified model of the processes attending the interaction of Fe^0-saturated peridotites with oxidized subducted crustal material in the deep zones of the Earth. Therefore, we believe that the basic regularities, found in this study, may reasonably be applied to natural, more complex systems. Taking into account the results of previous studies on diamond crystallization in different systems modeling natural media, we can discuss the possible effects of the individual components on the diamond-forming processes. First, it should be noted that the presence of alkalies will significantly decrease the temperature of generation of carbonate melts (37–39). A similar effect will be produced by H_2O-CO_2 fluids (40–42). It was experimentally shown that the addition of these components in the system significantly increases the diamond-forming ability of mantle fluids/melts (43, 44), acting in the oxidized conditions behind the redox front. Under reducing conditions, ahead of the redox front, where the diamond crystallized from Fe-C melt only, the presence of H_2O will lead to the inhibitory effect on the diamond-forming process (45). The addition of sulfur to the Fe-C system significantly decreases the melting temperature (46, 47). The produced melts are two immiscible liquids, with compositions similar to the Fe_3C and FeS. Sulfide melts are the least efficient diamond-forming media compared with carbonate, fluid, and carbonate-silicate-fluid environments (48, 49). The role of sulfides as reducing agents in the interaction with carbonates or CO_2 fluid, leading to the formation of elemental carbon (graphite or diamond), was experimentally demonstrated (35, 50).

The applicability of the redox mechanism is to the existence of deep zones in the Earth, containing native iron or iron carbides, and the possibility of subduction of carbonate minerals to these depths. In fact, there has been a growing body of evidence for the ultradeep subduction of carbonates and their participation in

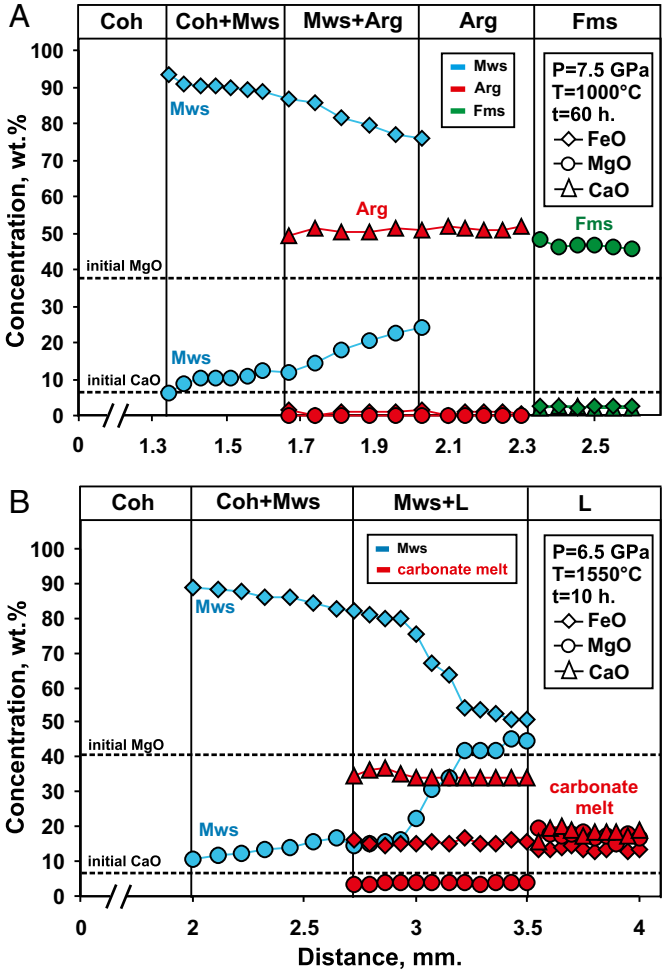

Fig. 4. Concentration profiles of FeO, MgO, and CaO across the redox front from the center to periphery of samples: (*A*) N 1541 (1,000 °C, 7.5 GPa); (*B*) N 1566 (1,550 °C, 6.5 GPa).

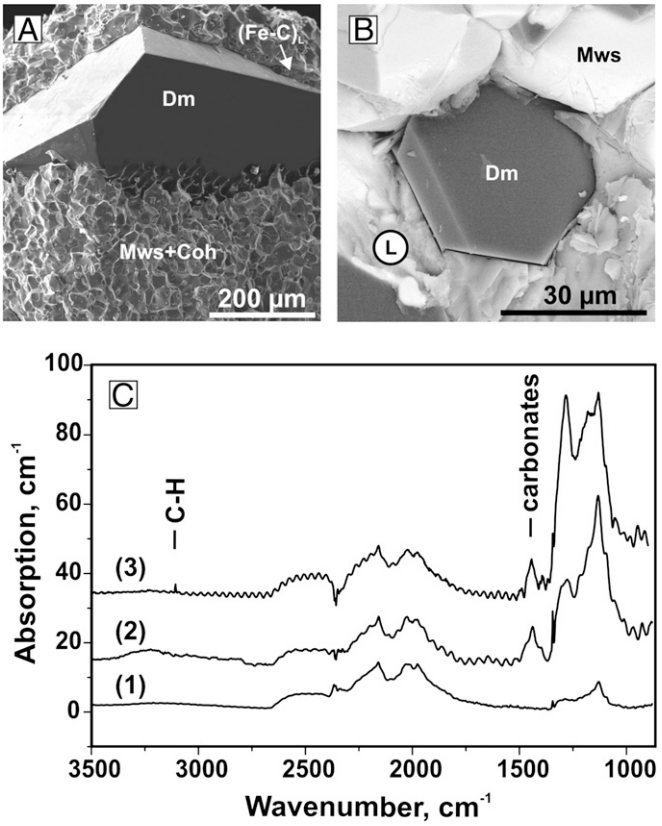

Fig. 5. SEM micrographs of crystallized diamonds and their typical infrared spectra: (*A*) diamond crystal from the metal-carbon melt (N 1566, 6.5 GPa, 1,550 °C); (*B*) diamond crystal from carbonate melt (N 1521, 7.5 GPa, 1,650 °C); (*C*) typical infrared absorption spectra of diamond crystals from (*1*) metal-carbon melt and (*2* and *3*) carbonate melt. The spectra have been vertically displaced for clarify.

the formation of diamonds. This evidence involves the discovery of inclusions in diamonds, consisting of carbonates in association with the superdeep phases $CaSiO_3$ or $MgO + MgSiO_3$, as well as some experimental and geochemical observations (51–54). Our results suggest that the Ca-rich carbonate melt, which forms through the carbonate–iron interaction and can be generated even in the absence of alkalis and H_2O, can be considered as a transmantle interstitial melt. High solubility of magnesiowustite in this carbonate melt produces a relatively low-melting temperature. The minimum temperature of nucleation and growth of diamonds in the carbonate melt, established in this study, is lower than that previously found for dry alkaline-carbonate melts (55).

Another important implication of the proposed redox front model is that it can explain the occurrence of inclusions in natural diamonds, with contrasting fO_2, which are traditionally considered as indicators of differing redox conditions (6, 21). The specifics of nucleation and growth of diamond under the carbonate–Fe^0 interaction may result in diamond formation at reduced conditions. Findings of central inclusions in diamond, represented by $Fe^0 + Fe_3C$ + graphite and FeO + graphite assemblages (21), indicate possible relevance of the studied interaction to the natural processes. On the other hand, diamonds, which are thought to originate from the lower part of the transition zone, contain primary alkali-earth carbonate inclusions (e.g., $CaCO_3$) (52). These diamonds could have formed from a Ca-rich carbonate melt, produced as a result of the subduction of oxidized material. We believe this to be a possible situation in nature, whereby diamonds nucleate in the metal melt and subsequently crystallize in the carbonate melt. In addition, it was determined that magnesiowustite formed in our experiments both at reduced and oxidized conditions, and its composition changes significantly as the redox front propagates. Therefore, we propose that the variations in the Mg/Fe ratio found for magnesiowustite inclusions in diamonds (53, 56) are directly related to the processes investigated in our experimental study.

A noteworthy finding in our study is highly contrasting concentrations of nitrogen impurities, exhibited by diamonds, crystallized at reduced and oxidized conditions in the course of a single redox interaction. This observation demonstrates that the partition coefficients of nitrogen are different for diamond crystallization in metal and carbonate melts and will require additional investigation. Nevertheless, even with the present results, it becomes clear that the changes in the crystallization conditions, brought about by the redox front propagation, can give rise to contrasting zonation in nitrogen and related defects distribution within a single diamond crystal. In general, the nitrogen content increases as the conditions evolve from reducing to oxidizing, with variations being on the order of ~1,000 ppm.

Our results show that the carbide, formed via the interaction of carbonate with carbon-free iron, is significantly depleted in the heavy-carbon isotope relative to the carbonate source. It is logical that the residual carbonate is enriched with ^{13}C. Thus, experimental data showed that nitrogen-poor diamonds grew in the reduced ^{13}C-depleted part of capsule, whereas nitrogen-rich diamonds occurred in the oxidized ^{13}C-enriched part of capsule. This general tendency of a simultaneous decrease of ^{13}C value and N abundance in diamonds fits well the "limit sector" correlation of N abundance and ^{13}C values in natural diamonds worldwide (57). One of the possible reasons of such observed interrelations of nitrogen and ^{13}C concentrations in natural diamonds can be a segregation of carbonate melt to form a diaper and its subsequent migration (38, 58) that can lead to the formation of contrasting domains of carbon isotopes in the Earth's low mantle. Taking into account the average magnitude of the fractionation of 6.5‰ and the nitrogen behavior (see above), the redox interaction can be considered as one of the mechanisms responsible for the complex compositional heterogeneity of natural diamonds (59–64).

Most of subducted carbonates have compositions of the $MgCO_3$-$CaCO_3$ series. Based on our results with such carbonate systems, we conclude that inclusions of Ca-rich carbonates, especially in association with magnesiowustite and other mantle minerals, are likely the products of the mechanism deduced from our experimentation.

Materials and Methods

Experiments were performed at pressures of 7.5 and 6.5 GPa, at temperatures of 1,000–1,650 °C and 1,350–1,600 °C, respectively, and with durations from 8 to 60 h, using a split-sphere multianvil apparatus (65). Details on the P-T calibration and accuracy of the measurements are given in ref. 66. Pt capsules of relatively large volume (6 and 10 mm in diameter at 7.5 and 6.5 GPa, respectively, 3.5–4.0 mm long) were used to enable a detailed study of the effects associated with the redox front propagation. The starting materials were mixtures of natural magnesite and dolomite, with bulk composition of $(Mg_{0.9}Ca_{0.1})CO_3$, powdered Fe^0 (99.999%), and presynthesized Fe_3C. A pellet of pressed iron or cohenite was placed into a carbonate container, which was then loaded into Pt capsules. This sandwich-type assembly of the reagents provided an fO_2 gradient over the samples and prevented the reaction between the metallic iron and Pt (Fig. S1). After runs, samples from different parts of capsules were studied using X-ray and electron microprobe analyses, optical and scanning electron microscopy, and Raman and infrared spectroscopy. Phase identification of run products was performed by X-ray diffraction (a DRON-3 diffractometer) and Raman spectroscopy. Raman spectra were measured using a Horiba J.Y. LabRAM HR800 spectrometer, with an Ar-ion laser (514 nm). An investigation of phase relations and measurements of energy dispersive spectra (EDS) of various phases were performed using a Tescan MIRA3 LMU SEM. The morphology of microdiamond crystals was studied using a Tescan MIRA3 LMU SEM and

an Olympus BX51 optical microscope. Infrared absorption spectra of diamonds were measured using a Bruker Vertex 70 FTIR spectrometer fitted with a Hyperion 2000 IR microscope. The isotopic analysis of carbon was performed using an isotope-ratio MAT-Delta mass spectrometer. Chemical compositions of synthetic phases were investigated using a Cameca Camebax-Micro microprobe. For electron microprobe analysis, polished sections of the samples were prepared. Mineral phases were analyzed with a focused electron beam of 1 μm diameter. Compositions of the quenched melt were defined using a defocused beam of 20–30 μm in diameter.

ACKNOWLEDGMENTS. We thank L. A. Taylor for useful comments and suggestions that helped to improve the manuscript. Insightful and constructive reviews by E. Ohtani and J. G. Liou are appreciated. Financial support from the Russian Foundation for Basic Research Grant 12-05-00740 and Siberian Branch of the Russian Academy of Sciences Integration Grant 31, and Deep Carbon Observatory is gratefully acknowledged.

1. Sobolev VS, Sobolev NV (1980) New evidence of the sinking to great depths of the eclogitized rocks of Earth crust. *Dokl Akad Nauk SSSR* 250(3):683–685.
2. Green DH, Eggins SM, Yaxley G (1993) Mantle dynamics: The other carbon-cycle. *Nature* 365(6443):210–211.
3. Dasgupta R, Hirschmann MM (2010) The deep carbon cycle and melting in Earth's interior. *Earth Planet Sci Lett* 298(1-2):1–13.
4. Harte B, Richardson S (2012) Mineral inclusions in diamonds track the evolution of a Mesozoic subducted slab beneath West Gondwanaland. *Gondwana Res* 21(1):236–245.
5. Walter MJ, et al. (2011) Deep mantle cycling of oceanic crust: Evidence from diamonds and their mineral inclusions. *Science* 334(6052):54–57.
6. Shirey SB, et al. (2013) Diamonds and the geology of mantle carbon. *Rev Mineral Geochem* 75(1):355–421.
7. Luth RW (1999) *Mantle Petrology*, eds Fei Y, Bertka CM, Mysen BO (Geochemical Society, St. Louis), pp 297–316.
8. Lord OT, Walter MJ, Dasgupta R, Walker D, Clark SM (2009) Melting in the Fe-C system to 70 GPa. *Earth Planet Sci Lett* 284(1-2):157–167.
9. Ryabchikov ID (2009) Mechanisms of diamond formation: Reduction of carbonates or partial oxidation of hydrocarbons. *Dokl Earth Sci* 429(1):1346–1349.
10. Boulard E, et al. (2011) New host for carbon in the deep Earth. *Proc Natl Acad Sci USA* 108(13):5184–5187.
11. Oganov AR, Hemley RJ, Hazen RM, Jones AP (2013) Structure, bonding and mineralogy of carbon at extreme conditions. *Rev Mineral Geochem* 75(1):47–77.
12. Woodland AB, Koch M (2003) Variation in oxygen fugacity with depth in the upper mantle beneath the Kaapvaal craton, Southern Africa. *Earth Planet Sci Lett* 214(1-2):295–310.
13. McCammon C, Kopylova MG (2004) A redox profile of the Slave mantle and oxygen fugacity control in the cratonic mantle. *Contrib Mineral Petrol* 148(1):55–68.
14. Stagno V, Ojwang DO, McCammon CA, Frost DJ (2013) The oxidation state of the mantle and the extraction of carbon from Earth's interior. *Nature* 493(7430):84–88.
15. Yaxley GM, Berry AJ, Kamenetsky VS, Woodland AB, Golovin AV (2012) An oxygen fugacity profile through the Siberian Craton: Fe K-edge XANES determinations of Fe3+/Sigma Fe in garnets in peridotite xenoliths from the Udachnaya East kimberlite. *Lithos* 140-141:142–151.
16. Rohrbach A, et al. (2007) Metal saturation in the upper mantle. *Nature* 449(7161): 456–458.
17. Rohrbach A, Schmidt MW (2011) Redox freezing and melting in the Earth's deep mantle resulting from carbon-iron redox coupling. *Nature* 472(7342):209–212.
18. Merlini M, et al. (2012) Structures of dolomite at ultrahigh pressure and their influence on the deep carbon cycle. *Proc Natl Acad Sci USA* 109(34):13509–13514.
19. Sobolev NV, Efimova ES, Pospelova LN (1981) Native iron in Yakutian diamonds and its paragenesis. *Soviet Geol Geophys* 22(12):18–21.
20. Stachel T, Harris JW, Brey GP (1998) Rare and unusual mineral inclusions in diamonds from Mwadui, Tanzania. *Contrib Mineral Petrol* 132(1):34–47.
21. Bulanova GP (1995) The formation of diamond. *J Geochem Explor* 53(1–3):1–23.
22. Kaminsky FV, Wirth R (2011) Iron carbide inclusions in lower-mantle diamond from Juina, Brazil. *Can Mineral* 49(2):555–572.
23. Jacob DE, Kronz A, Viljoen KS (2004) Cohenite, native iron and troilite inclusions in garnets from polycrystalline diamonds aggregates. *Contrib Mineral Petrol* 146(5):566–576.
24. Klein-BenDavid O, Izraeli ES, Hauri E, Navon O (2004) Mantle fluid evolution: A tale of one diamond. *Lithos* 77(1-4):243–253.
25. Schrauder M, Navon O (1993) Solid carbon dioxide in natural diamond. *Nature* 365(6441):42–44.
26. Sobolev NV, Logvinova AM, Efimova ES (2009) Syngenetic phlogopite inclusions in kimberlite-hosted diamonds: Implications for role of volatiles in diamond formation. *Russ Geol Geophys* 50(12):1234–1248.
27. Logvinova AM, Wirth R, Fedorova EN, Sobolev NV (2008) Nanometre-sized mineral and fluid inclusions in cloudy Siberian diamonds: new insights on diamond formation. *Eur J Mineral* 20(3):317–331.
28. Zedgenizov DA, Ragozin AL, Shatsky VS, Araujo D, Griffin WL (2011) Fibrous diamonds from the placers of the northeastern Siberian Platform: Carbonate and silicate crystallization media. *Russ Geol Geophys* 52(11):1298–1309.
29. Frost DJ, et al. (2004) Experimental evidence for the existence of iron-rich metal in the Earth's lower mantle. *Nature* 428(6981):409–412.
30. Frost DJ, McCammon CA (2008) The redox state of Earth's mantle. *Annu Rev Earth Planet Sci* 36:389–420.
31. Taylor L, Anand M (2004) Diamonds: Time capsules from the Siberian Mantle. *Chem Erde* 64(1):1–74.
32. Arima M, Kozai Y, Akaishi M (2002) Diamond nucleation and growth by reduction of carbonate melts under high-pressure and high-temperature conditions. *Geology* 30(8):691–694.
33. Siebert J, Guyot F, Malavergne V (2005) Diamond formation in metal-carbonate interactions. *Earth Planet Sci Lett* 229(3-4):205–216.
34. Pal'yanov YN, Sokol AG, Borzdov YM, Khokhryakov AF, Sobolev NV (2002) Diamond formation through carbonate-silicate interaction. *Am Mineral* 87(7):1009–1013.
35. Palyanov YN, et al. (2007) Reducing role of sulfides and diamond formation in the Earth's mantle. *Earth Planet Sci Lett* 260(1-2):242–256.
36. Strong HM, Chrenko RM (1971) Further studies on diamond growth rates and physical properties of laboratory-made diamond. *J Phys Chem* 75(12):1838–1843.
37. Grassi D, Schmidt MW (2011) Melting of carbonated pelites at 8-13 GPa: Generating K-rich carbonatites for mantle metasomatism. *Contrib Mineral Petrol* 162(1):69–191.
38. Litasov KD, Shatskiy A, Ohtani E, Yaxley GM (2013) Solidus of alkaline carbonatite in the deep mantle. *Geology* 41(1):79–82.
39. Shatskiy A, et al. (2013) The system K_2CO_3-$MgCO_3$ at 6 GPa and 900–1450°C. *Am Mineral* 98(8-9):1593–1603.
40. Foley SF (2011) A reappraisal of redox melting in the Earth's mantle as a function of tectonic setting and time. *J Petrol* 52(7-8):1363–1391.
41. Hirsmann M (2006) Water, melting, and the deep Earth H_2O cycle. *Annu Rev Earth Planet Sci* 34:629–653.
42. Wyllie PJ, Ryabchikov ID (2000) Volatile components, magmas, and critical fluids in upwelling mantle. *J Petrol* 41(7):1195–1206.
43. Palyanov YN, Shatsky VS, Sobolev NV, Sokol AG (2007) The role of mantle ultrapotassic fluids in diamond formation. *Proc Natl Acad Sci USA* 104(22):9122–9127.
44. Palyanov YN, Sokol AG (2009) The effect of composition of mantle fluids/melts on diamond formation processes. *Lithos* 112(S2):690–700.
45. Palyanov YuN, Borzdov YuM, Kupriyanov IN, Khokhryakov AF (2012) Effect of H_2O on diamond crystal growth in metal-carbon systems. *Cryst Growth Des* 12(11):5571–5578.
46. Dasgupta R, Buono A, Whelan G, Walker D (2009) High-pressure melting relations in Fe–C–S systems: Implications for formation, evolution, and structure of metallic cores in planetary bodies. *Geochim Cosmochim Acta* 73(21):6678–6691.
47. Deng L, Fei Y, Liu X, Gong Z, Shahar A (2013) Effect of carbon, sulfur and silicon on iron melting at high pressure: Implications for composition and evolution of the planetary terrestrial cores. *Geochim Cosmochim Acta* 114:220–233.
48. Palyanov YN, Borzdov YM, Khokhryakov AF, Kupriyanov IN, Sobolev NV (2006) Sulfide melts-graphite interaction at HPHT conditions: Implications for diamond genesis. *Earth Planet Sci Lett* 250(1-2):269–280.
49. Litvin YA (2012) Physicochemical formation conditions of natural diamond deduced from experimental study of the eclogite–carbonatite–sulfide–diamond system. *Geol Ore Deposits* 54(6):443–457.
50. Gunn SC, Luth RW (2006) Carbonate reduction by Fe–S–O melts at high pressure and high temperature. *Am Mineral* 91(7):1110–1116.
51. Stachel T, Harris JW, Brey GP, Joswig W (2000) Kankan diamonds (Guinea) II: Lower mantle inclusion parageneses. *Contrib Mineral Petrol* 140(1):16–27.
52. Brenker FE, et al. (2007) Carbonates from the lower part of transition zone or even the lower mantle. *Earth Planet Sci Lett* 260(1-2):1–9.
53. Bulanova GP, et al. (2010) Mineral inclusions in sublithospheric diamonds from Collier 4 kimberlite pipe, Juina, Brazil: Sbducted protoliths, carbonated melts and primary kimberlite magmatism. *Contrib Mineral Petrol* 160(4):489–510.
54. Walter MJ, et al. (2008) Primary carbonatite melt from deeply subducted oceanic crust. *Nature* 454(7204):622–625.
55. Pal'yanov YN, Sokol AG, Borzdov YM, Khokhryakov AF, Sobolev NV (1999) Diamond formation from mantle carbonate fluids. *Nature* 400(6743):417–418.
56. Hayman PC, Kopylova MG, Kaminsky FV (2005) Lower mantle diamonds from Rio Soriso (Juina area, Mato Grosso, Brazil). *Contrib Mineral Petrol* 149(4):430–445.
57. Cartigny P, Harris JW, Javoy M (2001) Diamond genesis, mantle fractionations and mantle nitrogen content: a study of delta C-13-N concentrations in diamonds. *Earth Planet Sci Lett* 185(1-2):85–98.
58. Dobretsov NL, Shatskiy AF (2012) Deep carbon cycle and geodynamics: The role of the core and carbonatite melts in the lower mantle. *Russ Geol Geophys* 53(11):1117–1132.
59. Galimov EM (1991) Istope fractionation related to kimberlite magmatism and diamond formation. *Geochim Cosmochim Acta* 55(6):1697–1708.
60. Boyd SR, Pineau F, Javoy M (1994) Modelling the growth of natural diamonds. *Chem Geol* 116(1–2):29–42.
61. Shiryaev AA, Izraeli ES, Hauri EH, Zakharchenko OD, Navon O (2005) Chemical, optical and isotopic investigation of fibrous diamonds from Brazil. *Russ Geol Geophys* 46(12):1185–1201.
62. Skuzovatov SY, Zedgenizov DA, Ragozin AL, Shatsky VS (2012) Growth medium composition of coated diamonds from the Sytykanskaya kimberlite pipe (Yakutia). *Russ Geol Geophys* 53(11):1197–1208.
63. Wiggers de Vries DF, et al. (2013) Micron-scale coupled carbon isotope and nitrogen abundance variations in diamonds: Evidence for episodic diamond formation beneath the Siberian Craton. *Geochim Cosmochim Acta* 100:176–199.
64. Howell D, et al. (2013) A spectroscopic and carbon-isotope study of mixed-habit diamonds: Impurity characteristics and growth environment. *Am Mineral* 98(1):66–77.
65. Palyanov YN, Borzdov YM, Khokhryakov AF, Kupriyanov IN, Sokol AG (2010) Effect of nitrogen impurity on diamond crystal growth processes. *Cryst Growth Des* 10(7):3169–3175.
66. Pal'yanov YN, Sokol AG, Borzdov YM, Khokhryakov AF (2002) Fluid-bearing alkaline-carbonate melts as the medium for the formation of diamonds in the Earth's mantle: An experimental study. *Lithos* 60(3-4):145–159.